Journal of Materials Chemistry A

Accepted Manuscript

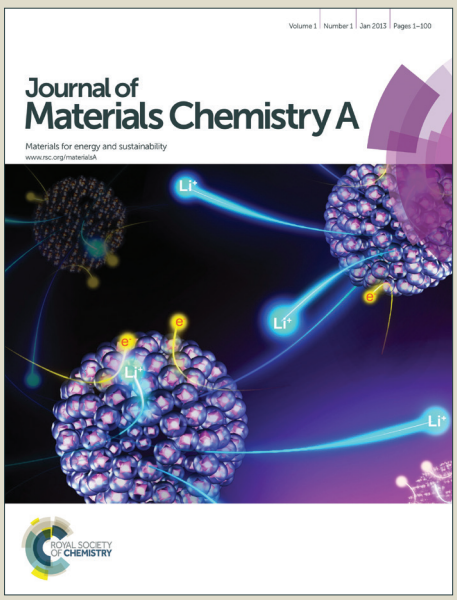

ROYAL SOCIETY OF CHEMISTRY

www.rsc.org/materialsA

Journal of
Materials Chemistry A

RSCPublishing

Paper

Highly Reduced VO_x Nanotube Cathode Materials with Ultra-high Capacity for Magnesium Ion Batteries

Cite this: DOI: 10.1039/x0xx00000x

Received ooth January 2012,
Accepted ooth January 2012

DOI: 10.1039/x0xx00000x

www.rsc.org/

Ryoung-Hee Kim, Ju-Sik Kim, Hyun-Jin Kim, Won-Seok Chang, Dong-Wook Han,* Seok-Soo Lee* and Seok-Gwang Doo

Here, we describe novel VO_x nanotubes with vanadium at various oxidation states ($V^{3+}/V^{4+}/V^{5+}$) as cathode materials for magnesium ion batteries. The VO_x nanotubes synthesized by a microwave-assisted hydrothermal process using an amine as an organic template show a high initial discharge capacity (~218 mA h g^{-1}) of more than 200 mA h g^{-1} and an outstanding cycling performance, which have not been previously reported for magnesium ion batteries. These improvements in the electrochemical performance of our VO_x nanotubes originate from the trivalent vanadium ions generated in the highly reduced VO_x nanotubes. The VO_x nanotubes with trivalent vanadium ions exhibit a lower charge transfer resistance at the electrode/electrolyte interfaces and superior cycling performance than the VO_x nanotubes containing vanadium ions of a higher oxidation state. We first suggest that the pristine oxidation state of the vanadium ions and the maintenance of a bonding structure on the surface of the VO_x nanotubes are the most important factors determining the magnesium insertion/extraction kinetics into/out of the VO_x nanotubes. Our findings offer a breakthrough strategy for achieving high-energy-density magnesium rechargeable batteries using VO_x nanotube cathode materials in combination with nanoarchitecture tailoring.

1 Introduction

The demand for renewable and sustainable energy sources has increased rapidly over the past few decades.[1,2] To meet this demand, extensive investigations and intensive research studies have been carried out on the development of wind and solar energy. By the same token, the interest in electricity storage systems (ESS) for the supply of the electricity generated by the renewable energy sources has also increased. Due to their high energy density and long cycle life, lithium ion batteries are the most promising candidates as ESS.[3-5] However, although lithium ion batteries have achieved great success as electrochemical power sources, challenges remain in their extensive use on account of the limited resources of lithium and safety issues involved.[6,7] From the points of view of cost and safety, magnesium rechargeable batteries are considered as a prospective next generation green energy system.[8,9]

As many researchers have mentioned, magnesium has several advantages in comparison to other materials. Importantly, magnesium is cheaper than lithium. In fact, magnesium is the fifth most abundant element on earth (after oxygen, silicon, aluminum, and iron).[10] If only the active material cost is considered, magnesium chemistry is more than four times cheaper than lithium-based chemistry. In addition, due to the bivalency of the magnesium ion, the specific volumetric capacity (3833 mAh/cc) of magnesium is higher than that of lithium (2046 mAh/cc).[8] Furthermore, the environmental friendliness of magnesium is adequate for ESS, which demand high safety.[11] However, the relatively poor electrochemical properties, such as low energy density and low working voltage, are challenges encountered in terms of the commercialization of Mg ion batteries.

One of the major issues that hinder the commercialization of magnesium ion batteries is the poor performance of the cathode. Owing to the strong polarization associated with the divalent character of the magnesium ion, the cathodic performance is mainly controlled by the slow kinetics of magnesium ion transport through the host materials.[8,11] Thus, considerable research has been directed toward reducing the energy barrier of the reversible Mg^{2+} movement thorough the cathode materials.[12,13] As noted by Novak et al., some oxides and sulfides have been proposed as possible active cathode materials.[14] Among various cathode materials for Mg ion batteries, vanadium oxides show great potential because of their high working voltage and non-toxicity.[15-17] Previous studies have reported V_2O_5/carbon composites[18] and Mg intercalated vanadium oxides including $Mg_xV_2O_5$ with high performance.[19] In general, a variety of nanostructured vanadium oxide cathode

materials demonstrated a superior electrochemical performance owing to their high reaction areas and short Mg ion migration pathways.[20,21] In particular, the nanotubes of vanadium oxide (VOx) have recently received much attention because of their favorable structure for Mg ion insertion and removal and high working voltage.[22] The VOx nanotube shows a layered structure with a large interlayer distance, which mainly consists of distorted edge-sharged VO_5 pyramids.[23] This novel structure allows Mg ions to access the interstitial and defect sites.

The methods typically employed for the synthesis of VO_x nanotubes involve the use of amine templates, which could improve the electrochemical performance. However, Jiang et al. demonstrated that the VO_x nanotubes synthesized by the hydrothermal method in the presence of amine precursors show a limited irreversible capacity (75 mA h g^{-1}) for the insertion of Mg ions in non-aqueous electrolytes.[24,25] Herein, we focused on the point that amine templates, such as octadecylamine and hexadecylamine, could play a role as a reductant when incorporated into VOx, leading to changes in the valance state of vanadium.[26,27] Considering that the insertion/removal reactions are accompanied by the partial reduction/oxidation of vanadium, the electrochemical properties of the VOx nanotubes can be tailored by the amount of amine templates, which affect the average oxidation state of vanadium.

The goal of the present study was to examine the electrochemical properties of the VOx nanotubes with different amount of amines for intercalation of Mg ions. The effect of the oxidation states of vanadium on the cycling ability was also examined.

2 Experimental

2.1 Synthesis and physicochemical characterization

VOx nanotubes were synthesized using a microwave-assisted hydrothermal method as recently reported by Li et al.[28] However, specific conditions, such as the precursor used and the reaction time, are different. Vanadium pentoxide (0.91 g) and octadecylamine (1.01 or 1.35 g) were dissolved in 5 mL of ethanol. After stirring, 25 mL of water was added. The precursor solution was mixed using a magnetic stirrer for more than 2 days to obtain a homogeneous sticky solution. The mixture was poured into a Teflon-lined autoclave and heated at 180 °C for 18 hours using microwaves (MARS5, CEM Co.). The resulting product was filtered and washed with ethanol several times. The final products were dried in a convection oven at 80 °C for more than 8 hours and heated in a vacuum oven at 100 °C for 2 hours to remove the residue solution. The structure of the VO_x nanotubes was characterized by XRD (Phillips X'Pert MPD, Cu Kα radiation). The scan speed was set to 3° per minute and the scanning was carried out between 3° and 50° at an applied potential of 40 kV and current of 40 mA. The morphology of the VO_x nanotubes was also observed by SEM (Hitachi S-5500) and transmission electron microscopy (TEM, FEI, Titan-80-300). X-ray photoelectron spectroscopy (XPS, Ulvac PHI, Versaprobe) was conducted to confirm the V2p binding energy of the samples. The cycled electrodes were transferred from an Ar-filled glove box to the XPS chamber using an air-proof chamber to avoid any contamination.

2.2 Electrochemical characterization

The VO_x electrodes were prepared by slurry casting. The weight ratio of VOx nanotube: carbon (Ketjen black): PVDF (polyvinyledene fluoride) in the slurry was 6:2:2. The resulting slurry was pasted onto an Al foil current collector and dried at 120 °C for 2 hours in a vacuum oven. After pressing, each dried paste was punched into a disc (1 cm in diameter). For the electrochemical tests, a Teflon three electrode cell was assembled in an Ar-filled glove box using a AZ31 magnesium alloy counter electrode and a $Ag/AgNO_3$ (0.1 N $AgNO_3$ in acetonitrile) reference electrode. $Mg(ClO_4)_2$ in deaerated acetonitrile solution (0.5 M) was used as the electrolyte. The water content in the electrolyte was less than 10 ppm. The cells were charged and discharged galvanostatically at 60 mAg^{-1} between 1.5 and 3.4 V (vs. Mg^{2+}/Mg) using a potentiostat (Solartron, SI 1287 ECI). The impedance spectra were measured at an open circuit in the galvanostatic mode over a frequency range of 0.1 Hz to 10 kHz using AC perturbation of 10 mV with a frequency response analyzer (Solartron, SI 1255 FRA) in conjunction with a potentiostat.

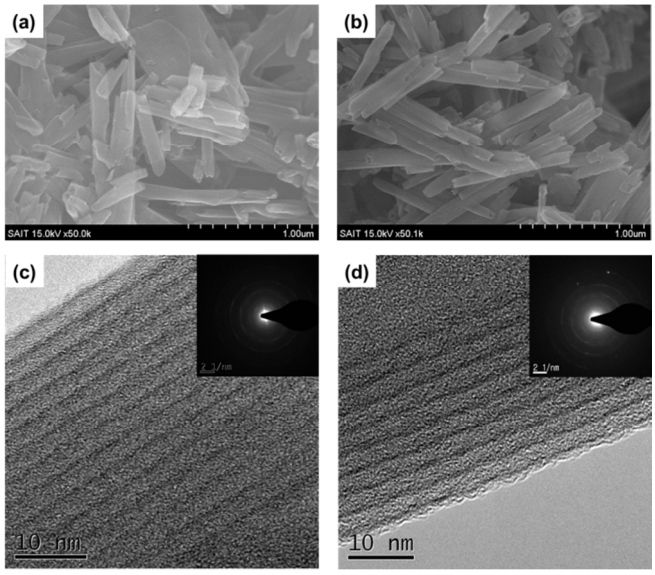

Fig. 1 Scanning electron microscopy (SEM) images of (a) LT-VO*x* and (b) HT-VO_x. High-resolution TEM (HR-TEM) images of (c) LT-VO_x and (d) HT-VO_x along with the corresponding selected area diffraction patterns (SADP).

3 Results and discussion

3.1 Morphology and crystal structure

Fig. 1a and 1b exhibit the scanning electron microscopy (SEM) images of vanadium oxide (VO_x) prepared via the microwave-assisted hydrothermal route using an amine as the organic templating molecule or the structure-directing agent. We denote VO_x obtained from relatively low and high concentrations of the amine template as LT-VO_x and HT-VO_x, respectively. The amine incorporated VO_x nanotubes showed a very special shape consisting of multiple layers of vanadium oxide separated by the templating molecules. The resulting VO_x nanotubes showed an average outer diameter of 80-100 nm and were 1-5 μm in length, as shown in the SEM images of LT-VO_x and HT-VO_x (Fig.S1). The similarity in the shape and size of the LT-VO_x and HT-VO_x nanotubes indicates that a minor difference in the amount of the amine template did not affect the morphology of the VO_x nanotubes. Further, the separation of the vanadium oxide layers was observed to mainly depend on the amine

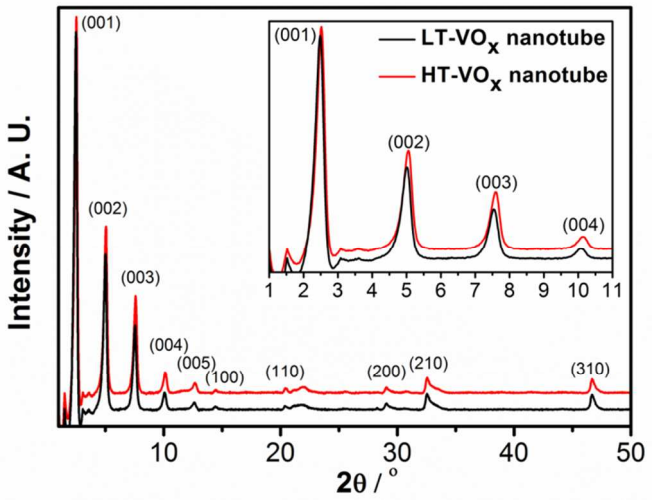

Fig. 2 X-ray powder diffraction (XRD) patterns of LT-VO_x and HT-VO_x.

length.[29] Fig. 1c and 1d show the high-resolution TEM (HR-TEM) images of LT-VO_x and HT-VO_x, respectively, along with the corresponding selected area diffraction patterns (SADP). We confirmed from the TEM images that crystalline VO_x uniformly formed within the thick nanotube walls, whereas the inner narrow core region seemed empty. This is in agreement with the open-ended structure of the VO_x nanotubes observed in the SEM images (Fig. 1a and 1b). Also, as in the case of the SEM images, there were no significant differences between the LT-VO_x and HT-VO_x nanotubes in terms of the microscopic structure and crystallinity, as shown in the HR-TEM and SADP images. The average distance between the VO_x layers in the nanotube walls was ~3.0 nm (Fig. 1c and 1d). These results indicate that the incorporated amine molecules could be embedded into the VO_x interlayers, which expanded the interlayer spaces and also facilitated the formation of the VO_x nanotubes.[30]

The crystal structure of the LT-VO_x and HT-VO_x nanotubes was verified by X-ray powder diffraction (XRD), and the results are presented in Fig. 2. The XRD patterns acquired from our VO_x nanotubes were found to be in agreement with the reference pattern of crystalline VO_x nanotubes.[31] The XRD patterns of HT-VO_x and LT-VO_x nanotubes did not show any notable differences in terms of the peak position and ratio. As shown in the inset of Fig. 2, the small-angle peak of HT-VO_x was marginally shifted toward higher angles, indicating a slight decrease in the layer spacing. However, the difference between the layer spacings calculated from the XRD results was less than ~0.1 nm. The XRD peaks at $2\theta > 10°$ can be attributed to the crystal structure within the VO_x layers; however, the peak with that highest intensity located at approximately ~2.5° corresponds to the (001) reflection and the d-spacing value coincides with the distance (~3.4 nm) between the VO_x layers determined by the HR-TEM analyses of both the VO_x samples.

3.2 Electrochemical properties

The initial galvanostatic (0.2 C, 1 C-rate = 300 mA h g^{-1}) voltage profiles of LT-VO_x and HT-VO_x measured in the range 1.5–3.4 V (vs. Mg^{2+}/Mg) are shown in Fig. 3a. The initial discharge capacity was higher for LT-VO_x (~230 mA h g^{-1}) than for HT-VO_x (~218 mA h g^{-1}). To the best of our knowledge, this is the first result to demonstrate the insertion of

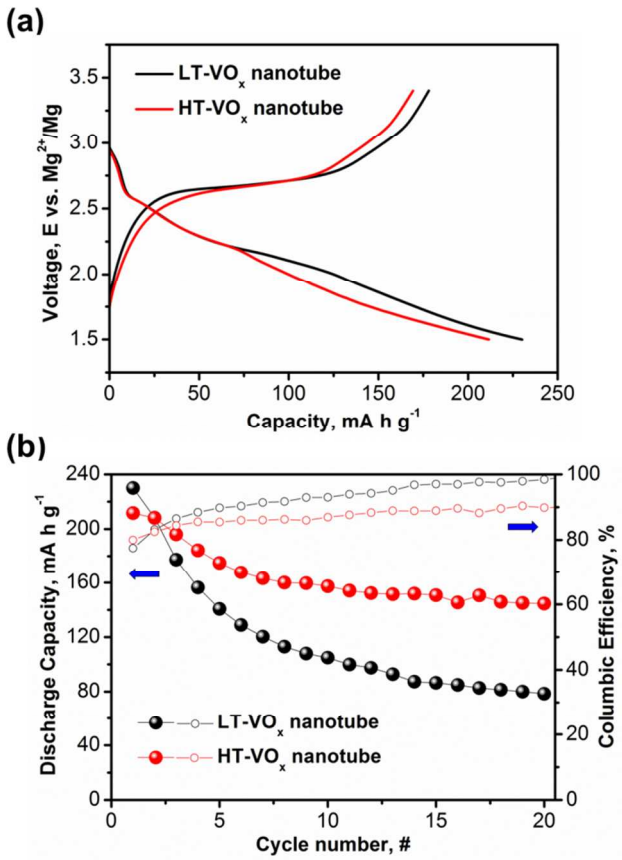

Fig. 3 (a) Initial galvanostatic (0.2 C, 1 C-rate = 300 mA h g^{-1}) voltage profiles and (b) cycling performance and columbic efficiency of LT-VO_x and HT-VO_x.

Mg^{2+} ions into the VO_x host crystal structure at a capacity >200 mA h g^{-1}. According to Jiao et al., the VO_x nanotubes obtained by a sol-gel reaction followed by hydrothermal treatment achieved ~75 mA h g^{-1} of its initial discharge capacity even at a sufficiently low current density of 5 mA g^{-1}.[25] Although the initial discharge/charge capacities of HT-VO_x was slightly lower than the values shown by LT-VO_x, the cycling performance of the HT-VO_x was superior than that of LT-VO_x, as observed in Fig. 3b. The two materials exhibited entirely different capacity fading properties. The discharge capacity of LT-VO_x decreased rapidly after the first cycle and the capacity retention dropped below 70% after four cycles. However, HT-VO_x nanotubes exhibited a high discharge capacity of ~150 mA h g^{-1}, corresponding to ~70.8% of its initial discharge capacity after 20 cycles. The enhanced capacity retention property of HT-VO_x might be partly ascribed to the structural stability associated with the maintenance of the layer spacing to the facile movement of Mg^{2+} ions. Meanwhile, The columbic efficiency of VO_x nanotubes was closely related with Mg^{2+} ions utilization; i.e. the discharge capacity and columbic efficiency of the HT-VO_x measured after 20 cycles were almost identical to those of LT-VO_x measured after 4 cycles, as observed in Fig.3b. However, the correlation between the variation in the amount of amine molecules and the insertion/extraction characteristics of Mg^{2+} ions into/from VO_x nanotubes is yet to be completely understood.

3.3 X-ray photoelectron spectroscopy (XPS) and ex-situ transmission electron microscopy (TEM) analyses

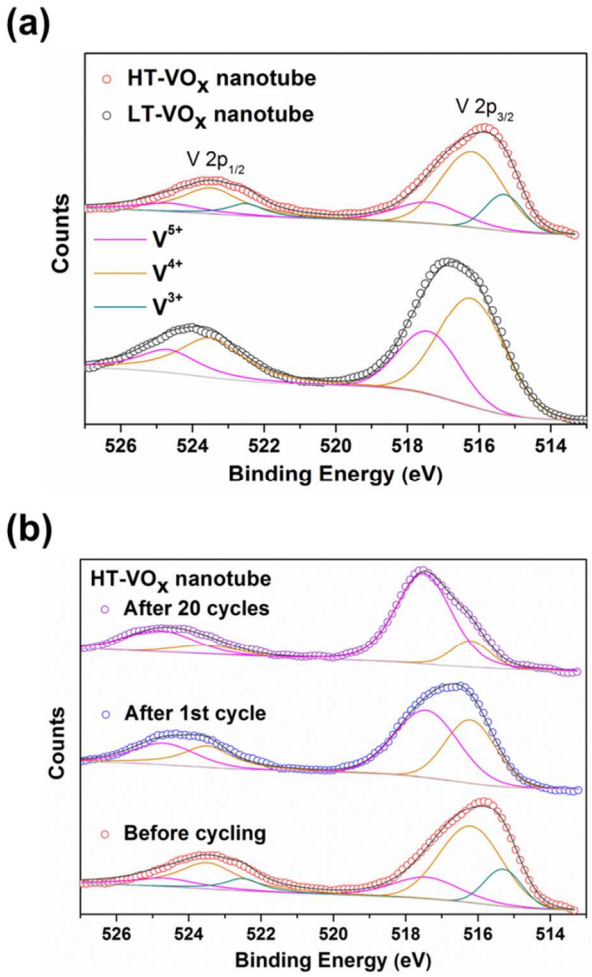

Fig. 4 (a) X-ray photoelectron spectroscopy (XPS) profiles of LT-VO_x and HT-VO_x measured before cycling. (b) XPS profiles of HT-VO_x after the first and 20th cycle.

To understand the origin of the improvement in the electrochemical performance of HT-VO_x nanotubes, we compared the X-ray photoelectron spectroscopy (XPS) profiles of LT-VO_x and HT-VO_x acquired before and after cycling. XPS is one of the most effective tools for determining the chemical bonding structure on the surface of materials.[32] The deconvoluted V 2p XPS core peaks of the LT-VO_x and HT-VO_x nanotubes before cycling (Fig. 4a) showed that LT-VO_x with mixed valencies of V consisted of V^{4+} (516.2 eV) and V^{5+} (517.4 eV) with the V^{5+}/V^{4+} ratio equal to ~0.53. In contrast, the amounts of V^{4+} and V^{5+} were diminished and a new V 2p XPS core peak (at 515.3 eV) for V^{3+} appeared in the case of HT-VO_x. An intrinsic partial reduction of vanadium in the VO_x nanotubes from V^{5+} to V^{4+} caused by the presence of amines has been previously reported.[29] It is known that amines act as a reducing agent during the synthesis of the nanotubes; however, the reduction from the initial oxidation state of V^{4+} to V^{3+} has been demonstrated for the first time in the present study. In addition, we note from the V 2p XPS spectra of the HT-VO_x nanotubes acquired after the first and 20th cycles (Fig. 4b) that the reduced V^{3+} on the surface of the HT-VO_x nanotubes disappeared after the 1st cycle and then the amount of V^{5+} abruptly increased after the subsequent cycles, indicating the occurrence of irreversible electrochemical redox reactions ($V^{5+} \Leftrightarrow V^{4+}$ and/or $V^{4+} \Leftrightarrow V^{3+}$). In particular, the valence state of vanadium of LT-VO_x was totally changed to 5+ after only 1 cycle (Fig.S2). Hence, a decrease in the initial oxidation state of vanadium and maintenance of the bonding structure on the surface of the VO_x nanotubes seem to positively affect the cycling performance of the VO_x nanotubes. The extent of vanadium reduction during the synthesis of the VO_x nanotubes has been recognized as the driving force for the rolling up of the VO_x sheets to form nanotubes.[30] Therefore, Therefore, the more the reduction in the vanadium oxidation states, the stronger the VO_x sheets roll into nanotubes. As shown in Fig. 5, the unique rolled structure was almost not observed in LT-VO_x after 20 cycles (Fig. 5a); on the other hand, the layered structure and rolled-tube shape was maintained after 20 cycles in HT-VO_x (Fig. 5b). Moreover, a reduction in the oxidation state of vanadium changes a portion of the VO_4 tetrahedron (V^{5+}) or VO_5 square pyramid (V^{5+} mixed with V^{4+}) in the VO_x to VO_6 octahedrons (V^{3+}).[33,34] Taking into consideration the larger ionic size and higher coordination number of V^{3+} in comparison to V^{4+} and V^{5+}, the VO_6 octahedron can expand the interstitial sites consisting of the VO_4 tetrahedron and VO_5 square pyramid, which might enhance the Mg^{2+} mobility in the crystal structure of VO_x. Therefore, it can be concluded that the existence of V^{3+} in the VO_x nanotubes is advantageous for their use as electrode materials in magnesium ion batteries.

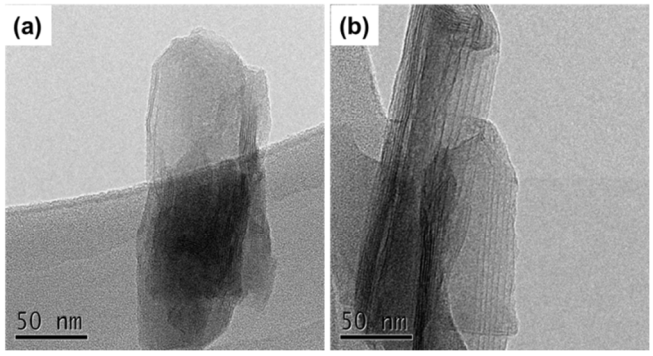

Fig. 5 TEM images of (a) LT-VO_x and (b) HT-VO_x after 20 cycles.

3.4 Electrochemical impedance spectroscopy (EIS) analysis

The electrochemical impedance spectroscopy (EIS) measurements were performed on LT-VO_x and HT-VO_x, and their EIS spectra along with an appropriate equivalent circuit model are shown in Fig. 6. The Nyquist plots of the materials showed only one semicircle in the high-middle frequency region, corresponding to charge transfer resistance ($R_{ct,VOx}$), in addition to a typical sloping Warburg line (Z_w) in low

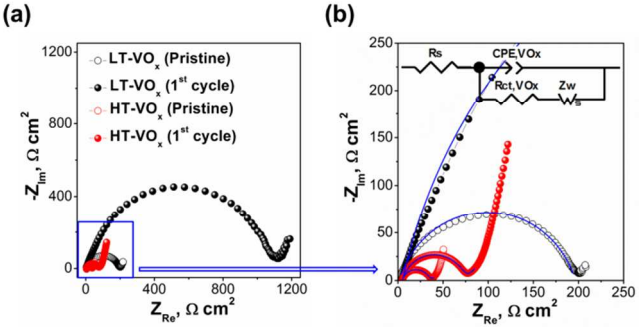

Fig. 6 The results of the electrochemical impedance spectroscopy (EIS) analysis of LT-VO_x and HT-VO_x before cycling and after the first cycle.

frequency region. As a result, the HT-VO_x sample showed a lower charge transfer resistance (~29.2 Ω cm^2) than LT-VO_x (~152.8 Ω cm^2) before cycling. After the first cycle, while the charge transfer resistance of the LT-VO_x abruptly increased to more than 10^3 Ω cm^2, the HT-VO_x featured a low charge transfer resistance of ~69.5 Ω cm^2. Four-point probe electrical measurements indicated that the electrical conductivity of the VO_x nanotubes decreased with an increase in the amount of the amines. This is because the electrical conductivity of the amine is several orders of magnitude lower than that of the VO_x nanotubes. Therefore, we conclude that a reduction in the charge transfer resistance of the VO_x nanotubes as a function of the amine content is associated with the facile Mg^{2+} ion migration through the electrode/electrolyte interface because the charge transfer resistance estimated from the semicircle is attributed to mixed ionic (Mg^{2+}) and electronic conduction through the interface. The improved cycle ability (Fig. 3b) and diminished charge transfer resistance of HT-VO_x compared to LT-VO_x probably stem from an enhancement of the Mg^{2+} mobility induced by the formation of large clusters of V^{3+}-O in the crystal structure of the VO_x nanotubes.

Conclusions

In summary, we succeeded in preparing VO_x nanotubes through a microwave-assisted hydrothermal route using amine as an organic templating molecule or a structure-directing agent. The VO_x nanotubes obtained showed an average outer diameter of 80-100 nm and a length of 1-5 μm and their morphology was not affected by the amount of the incorporated amine. However, unlike LT-VO_x consisting of V^{4+} and V^{5+}, further reduction in the initial oxidation state of vanadium to +3 was observed in HT-VO_x. In addition, HT-VO_x showed an improved cycling performance (discharge capacity of ~150 mA h g^{-1} after 20 cycles) in comparison to LT-VO_x. The enhanced electrochemical performance of HT-VO_x seems to be closely related to the presence of V^{3+}. The relatively low binding energy of V in HT-VOx exerts a decisive effect on the structural stability and/or reduced charge transfer resistance at the VO_x nanotube/electrolyte interfaces. An enhancement in the Mg^{2+} mobility induced by the formation of large V^{3+}-O clusters in the crystal structure of the VO_x nanotubes probably improved the kinetics of Mg^{2+} migration, thereby diminishing the charge transfer resistance at the interfaces.

Acknowledgements

The authors gratefully acknowledge D. J. Yun for XPS measurements.

Notes and references

Energy Lab, Samsung Advanced Institute of Technology (SAIT), Samsung Electronics Co., 130 Samsung-ro, Yeongtong-gu, Suwon-si, Gyeonggi-do, 443-803, Republic of Korea. E-mail: dongwook.han@samsung.com; seoksoo.lee@samsung.com

1 J. Liu, *Adv. Funct. Mater.*, 2013, **23**, 924.
2 C. Liu, F. Li, M. Lai-Peng and H.-M. Cheng, *Adv. Mater.*, 2010, **22**, E28.
3 J.-M. Tarascon and M. Armand, *Nature*, 2001, **414**, 359.
4 V. Etacheri, R. Marom, R. Elazari, G. Salitra and D. Aurbach, *Energy Environ. Sci.*, 2011, **4**, 3243.
5 Z. Gong and Y. Yang, *Energy Environ. Sci.*, 2011, **4**, 805.
6 B. Dunn, H. Kamath and J.-M. Tarascon, *Science*, 2011, **334**, 928.
7 Z. Yang, J. Zhang, M. C. W. Kintner-Meyer, X. Lu, D. Choi, J. P. Lemmon and J. Liu, *Chem. Rev.*, 2011, **111**, 3577.
8 D. Aurbach, Z. Lu, A. Schechter, Y. Gofer, H. Gizbar, R. Turgeman, Y. Cohen, M. Moshkovich and E. Levi, *Nature*, 2000, **407**, 724.
9 I. Shterenberg, M. Salama, Y. Gofer, E. Levi and D. Aurbach, *MRS Bull.*, 2014, **39**, 453.
10 H. D. Yoo, I. Shterenberg, Y. Gofer, G. Gershingsky, N. Pour and D. Aurbach, *Energy Environ. Sci.*, 2013, **6**, 2265.
11 H. S. Kim, T. S. Arthur, G. D. Allred, J.Zajicek, J. G. Newman, A. E. Rodnyansky, A. G. Oliver, W. C. Boggess and J. Muldoon, *Nat. Commun.*, 2011, **2**, 427.
12 B. Liu, T. Luo, G. Mu, X. Wang, D. Chen and G. Shen, *ACS Nano*, 2013, **7**, 8051.
13 Y. Liu, L. Jiao, Q. Wu, Y. Zhao, K. Cao, H. Liu, Y. Wang and H. Yuan, *Nanoscale*, 2013, **5**, 9562.
14 P. Novák, R. Tuhof and O. Haas, *Electrochim. Acta*, 1999, **45**, 351.
15 T. D. Gregory, R. J. Hoffman and R. C. Winterton, *J. Electrochem. Soc.*, 1990, **137**, 775.
16 M. Martin, O. J. Besenhard, M. E. Spahr and P. Novák, *Adv. Mater.*, 1998, **10**, 725.
17 N. A. Chernova, M. Roppolo, A. C. Dillon and M. S. Whittingham, *J. Mater. Chem.*, 2009, **19**, 2526.
18 D. Imamura, M. Miyayama, M. Hibino and T. Kudo, *J. Electrochem. Soc.*, 2003, **150**, A753.
19 S. H. Lee, R. A. DiLeo, A. C. Marschilok, K. J. Takeuchi and E. S. Takeuchi, *ECS Electrochem. Lett.*, 2014, **3**, A87.
20 J. W. Lee, S. Y. Lim, H. M. Jeong, T. H. Hwang, J. K. Kang and J. W. Choi, *Energy Environ. Sci.*, 2012, **5**, 9889.
21 Q. Qu, Y. Zhu, X. Gao and Y. Wu, *Adv. Energy Mater.*, 2012, **2**, 950.
22 C. Cui, G. Wu, J. Shen, B. Zhou, Z. Zhang, H. Yang and S. She, *Electrochim. Acta*, 2010, **55**, 2536.
23 G. R. Patzke, F. Krumeich and R. Nesper, *Angew. Chem. Int. Ed.*, 2002, **41**, 2446.
24 L. Jiao, H. Yuan, Y. Wang, J. Cao and Y. Wang, *Electrochem. Commun.*, 2005, **7**, 431.
25 L. Jiao, H. Yuan, Y. Si, Y. Wang, J. Cao, X. Gao, M. Zhao, X. Zhou and Y. Wang, *J. Power Sources*, 2006, **156**, 673.
26 M. Wörle, F. Krumeich, F. Bieri, H. J. Muhr and R. Nesper, *Z. Anorg. Allg. Chem.*, 2002, **628**, 2778.
27 J. Livage, *Materials*, 2010, **3**, 4175.
28 J. M. Li, K. H. Chang, T. H. Wu and C. C. Hu, *J. Power Sources*, 2013, **224**, 59.
29 F. Krumeich, H. J. Muhr, M. Niederberger, F. Bieri, B. Schnyder and R. Nesper, *J. Am. Chem. Soc.*, 1999, **121**, 8324.
30 L. I. Vera-Robles and A. Campero, *J. Phys. Chem. C*, 2008, **112**, 19930.
31 M. Niederberger, H. J. Muhr, F. Krumeich, F. Bieri, D. Gunther and R. Nesper, *Chem. Mater.*, 2000, **12**, 1995.
32 W. H. Kan, M. Chen, J.-S. Bae, B.-H. Kim and V. Thangadurai, *J. Mater. Chem. A*, 2014, **2**, 8736.
33 S. A. Corr, M. Grossman, J. D. Furman, B. C. Melot, A. K. Cheetham, K. R. Heier and R. Seshadri, *Chem. Mater.*, 2008, **20**, 6396.

34 P. Y. Zavalij and M. S. Whittingham, *Acta Crystallogr. B*, 1999, **55**, 627.

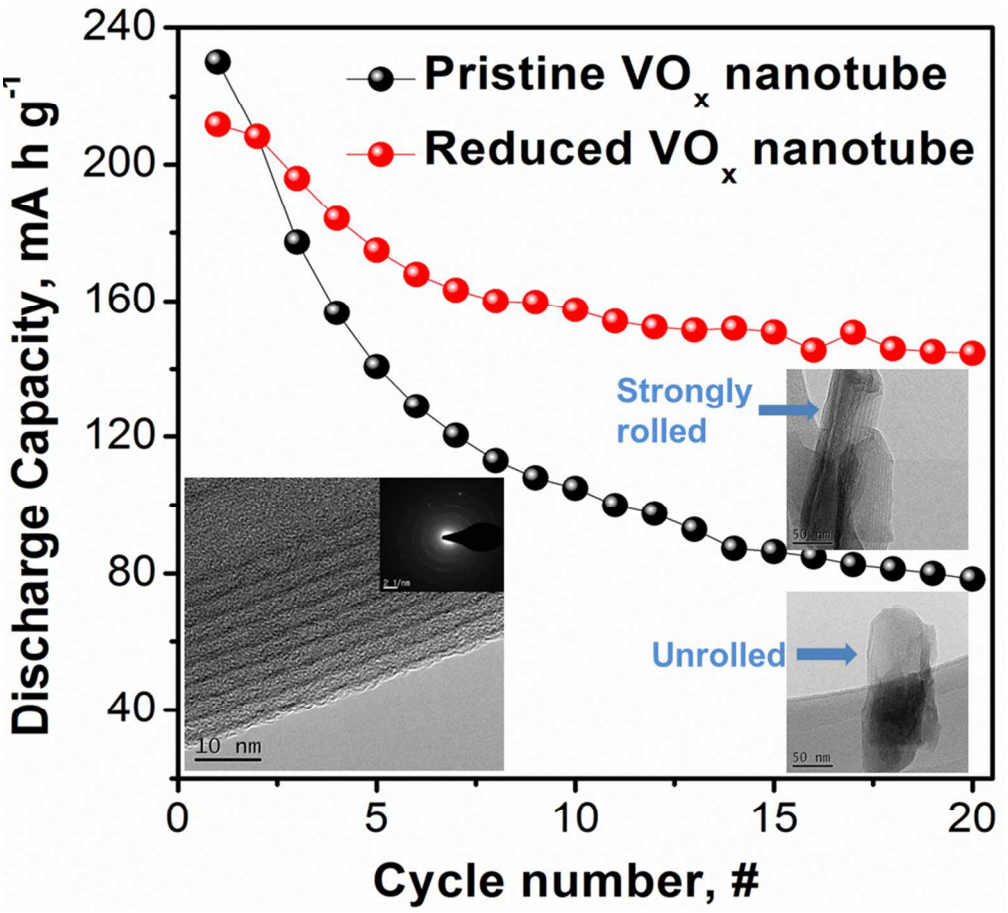

The remarkable cycling performance of VOx nanotubes originate from the trivalent vanadium ions generated in the highly reduced VOx nanotubes.
165x149mm (150 x 150 DPI)